THE MICROSCOPE • Vol. 68:3/4, pp 99–110, 2020

A Comprehensive Suite of *d-θ* Look-Up Tables for Indexing Zone-Axis SAED Patterns of Amphibole Asbestos and Related Minerals

Shu-Chun Su, Ph.D.
Technical Expert, National Voluntary Laboratory Accreditation Program
National Institute of Standards and Technology[1]

ABSTRACT

The analysis of asbestos minerals below optical resolution is conducted by the analytical transmission electron microscopy (TEM). The Asbestos Hazard Emergency Response Act (AHERA) protocol mandates the measurement of three properties: the morphology by the TEM imaging, the elemental composition by the energy-dispersive X-ray spectroscopy (EDS), and the crystal structure by the zone-axis selected area electron diffraction (SAED). After the acquisition of a zone-axis SAED pattern with EDS-derived mineral identity, the practical and effective methodology of its indexing and interpretation is the comparison of the measured (observed) values of the *d*-spacings of two intersecting direct lattice planes and their interplanal angle against the reference values in pre-calculated *d*-spacing and interplanal angle look-up tables (*d-θ* table) based on the mineral's unit cell parameters and symmetry. This paper presents a suite of hitherto most comprehensive *d-θ* look-up tables (more than 800 pages and 36,000 zone axes) for five regulated amphiboles (anthophyllite, grunerite, riebeckite, tremolite, and actinolite), three non-regulated ones (winchite, richterite, and cummingtonite), and talc, which could be confused with the regulated anthophyllite to facilitate the analysis of zone-axis SAED patterns. The procedure of using the *d-θ* look-up table is illustrated by two examples. Issues relevant to applications of *d-θ* table are also discussed.

Keywords: transmission electron microscopy (TEM), energy-dispersive X-ray spectroscopy (EDS), selected area electron diffraction (SAED), diffraction camera constant, indexing, zone-axis, *d*-spacing, interplanar angle, asbestos, amphibole, amosite, grunerite, crocidolite, riebeckite, tremolite, actinolite, anthophyllite, winchite, richterite, cummingtonite, talc, Libby (Montana), Miller index, Weiss zone law

Scan this QR code to access the article abstract and *d-θ* look-up tables (PDF files) for anthophyllite, grunerite, riebeckite, tremolite, actinolite, winchite, richterite, cummingtonite, and talc on www.mccroneinstitute.org[2].

INTRODUCTION

The identification of airborne asbestos minerals by the AHERA protocol is based on three properties: morphology by transmission electronic microscopy (TEM) imaging, elemental composition analysis by energy-dispersive X-ray spectroscopy (EDS), and crystal structure by the zone-axis selected area electron diffraction (SAED) pattern analysis. The purpose of zone-axis SAED pattern analysis is to further confirm the mineral's identity, which is initially established through TEM imaging and EDS analysis, by demonstrating that the characteristics of its diffraction pattern conforms to that mineral's crystal structure. The SAED analysis is consisted of two steps: indexing, which is to determine the Miller index (1) of the diffraction spots in the pattern as well as that of the resulting zone axis, and interpretation, which is to draw conclusion whether the indexed SAED pattern conforms to the crystal structure of the identified mineral.

The most effective methodology of indexing and interpretation is through the comparison of the mea-

[1]100 Bureau Drive, Gaithersburg, MD 20899; shuchunsu@gmail.com
[2]http://www.mccroneinstitute.org/v/1559/The-Microscope-Volume-68-ThirdFourth-Quarters-2020

Table 1. The Crystallographic Properties of Five AHERA Amphiboles, Winchite, Richterite, Talc, and Cummingtonite

Mineral	Crystallographic System	*a b c*	*α*	*β*	*γ*	Space Group	Diffraction Constraints
Tremolite	Monoclinic	$a \neq b \neq c$	90°	>90°	90°	C2/m	(h+k) = 2n
Actinolite	Monoclinic	$a \neq b \neq c$	90°	>90°	90°	C2/m	(h+k) = 2n
Grunerite	Monoclinic	$a \neq b \neq c$	90°	>90°	90°	C2/m	(h+k) = 2n
Riebeckite	Monoclinic	$a \neq b \neq c$	90°	>90°	90°	C2/m	(h+k) = 2n
Anthophyllite	Orthorhombic	$a \neq b \neq c$	90°	90°	90°	Pnma	(hk0): h = 2n (0kl): (k+l) = 2n
Winchite	Monoclinic	$a \neq b \neq c$	90°	>90°	90°	C2/m	(h+k) = 2n
Richterite	Monoclinic	$a \neq b \neq c$	90°	>90°	90°	C2/m	(h+k) = 2n
Cummingtonite	Monoclinic	$a \neq b \neq c$	90°	>90°	90°	C2/c	(h+k) = 2n
Talc	Triclinic	$a \neq b \neq c$	≠90°	≠90°	≠90°	C-1	(h+k) = 2n

sured (observed) values of the *d*-spacing of two sets of intersecting lattice planes and their interplanal angle θ against the respective reference values in pre-calculated *d*-θ tables based on the mineral's unit cell parameters and symmetry.

Whereas the intensity of diffraction spots is determined primarily by the crystal's chemical composition, the geometry or the spatial distribution of diffraction spots is entirely governed by cell parameters and symmetry of the direct lattice, i.e., the lengths *a, b, c* of the three crystallographic axes *x, y, z*, the interaxial angles between them α (*y*^*z*), *b* (*x*^*z*), γ (*x*^*y*), and its space group (2). This paper presents a suite of d-θ look-up tables for nine minerals: the five regulated amphiboles (3), three non-regulated ones (winchite, richterite, and cummingtonite), and talc, which could be confused with the regulated anthophyllite because of similarities in composition and structure. Their crystallographic properties are summarized in Table 1.

The space group determines the condition of the systematic extinction or absence, i.e., diffraction spots that are not to appear in the patterns. For SP = C2/m, C2/c and C-1, only (h+k) = 2n diffractions are permitted. Any diffraction spots with (h+k) ≠ 2n are extinct or absent in the pattern. For SP = Pnma, only h = 2n diffractions for (hk0) and (k+l) = 2n for (0kl) are allowed. Any h ≠ 2n diffraction for (hk0) and (k+l) ≠ 2n diffraction for (0kl) are extinct or absent in the pattern.

PRE-CALCULATED *d*-θ LOOK-UP TABLES

In theory, it is possible to solve a zone-axis SAED pattern by a dedicated computer program, e.g., *Single-Crystal* (4). However, it is inefficient and difficult to do so. In practice, after the initial establishment of the mineral's identity by morphology and chemistry, the only practical way to solve an unknown pattern is to compare its measured (observed) values of the *d*-spacings of two intersecting lattice planes and their interplanal angle against the corresponding reference values in pre-calculated *d*-spacing and interplanal angle reference tables or *d*-θ look-up tables for that particular mineral. As shown in Table 2, a comprehensive suite of *d*-θ tables for the amphiboles and talc listed in Table 1 can be generated using the algorithms described below.

1) The algorithms of *d*-θ table generation (14, 1).

The calculations of all three parameters, *d*, θ, and the angle between the zone axis or the electron beam to [0 0 1] or *c*-axis, can be accomplished by using the second-order Metric Tensor [*MT*] from the direct lattice parameters *a, b, c,* α, β, γ, and its inverse $[MT]^{-1}$ or [*MT*]* from the reciprocal lattice parameters *a**, *b**, *c**, α*, β*, γ*.

$$[MT] = \begin{bmatrix} a*a & a*b & a*c \\ b*a & b*b & b*c \\ c*a & c*b & c*c \end{bmatrix} \begin{bmatrix} a^2 & ab\cos\gamma & ac\cos\beta \\ ab\cos\gamma & b^2 & bc\cos\alpha \\ ac\cos\beta & bc\cos\alpha & c^2 \end{bmatrix}$$

and

$$[MT]^* = \begin{bmatrix} a^{*2} & a^*b^*\cos\gamma^* & a^*c^*\cos\beta^* \\ a^*b^*\cos\gamma^* & b^{*2} & b^*c^*\cos\alpha^* \\ a^*c^*\cos\beta^* & b^*c^*\cos\alpha^* & c^{*2} \end{bmatrix}$$

where $Vol = (\det[MT])^{1/2}$

$a^* = bc\sin\alpha/Vol$

$b^* = ac\sin\beta/Vol$

$c^* = ab\sin\gamma/Vol$

Table 2. The Crystallographic Parameters and [*MT*] Plus [*MT*]* of the Nine Minerals

Asbestos	Anthophyllite	Grunerite	Riebeckite	Tremolite	Actinolite	Winchite	Richterite	Cummingtonite	Talc
Reference	5. Warren, et al. (1930)	6. Finger (1969)	7. Hawthorne (1978)	8. Ballirano, et al. (2008)	9. Evans, et al. (1998)	10. Wylie, et al. (2000)	11. Ventura, et al. (1993)	12. Fisher (1966)	13. Perdikatsis, et al. (1981)
System	Orthorhombic	Monoclinic	Monoclinic	Monoclinic	Monoclinic	Monoclinic	Monoclinic	Monoclinic	Triclinic
Space Group	Pnma	C2/m	C2/m	C2/m	C2/m	C2/m	C2/m	C2/m	C –1
Diffraction Allowed	(hk0): h=2n (0kl): (k+l)=2n	(h+k)=2n	(h+k)=2n	(h+k)=2n	(h+k)=2n	(h+k)=2n	(h+k)=2n	(h+k)=2n	(h+k)=2n
***a* (Å)**	18.500	9.564	9.769	9.842	9.886	9.855	10.030	9.510	5.290
***b* (Å)**	17.900	18.393	18.048	18.059	18.171	18.032	18.415	18.190	9.173
***c* (Å)**	5.280	5.339	5.335	5.279	5.297	5.288	5.234	5.330	9.460
α (°)	90.000	90.000	90.000	90.000	90.000	90.000	90.000	90.000	90.460
β (°)	90.000	101.892	103.590	104.732	104.610	104.540	104.970	101.900	98.680
γ (°)	90.000	90.000	90.000	90.000	90.000	90.000	90.000	90.000	90.090
a*	0.0541	0.1068	0.1053	0.1051	0.1045	0.1048	0.1032	0.1075	0.1912
b*	0.0559	0.0544	0.0554	0.0554	0.0550	0.0555	0.0543	0.0550	0.1090
c*	0.1894	0.1914	0.1928	0.1959	0.1951	0.1954	0.1978	0.1917	0.1069
α*	90.0000	90.0000	90.0000	90.0000	90.0000	90.0000	90.0000	90.0000	89.5264
β*	90.0000	78.1080	76.4100	75.2680	75.3900	75.4600	75.0300	78.1000	81.3193
γ*	90.0000	90.0000	90.0000	90.0000	90.0000	90.0000	90.0000	90.0000	89.8406
V	1748.4720	919.0147	914.2833	907.3779	920.7771	909.6096	933.9229	902.2050	453.7806
V*	0.0006	0.0011	0.0011	0.0011	0.0011	0.0011	0.0011	0.0011	0.0022
G11	342.2500	91.4739	95.4334	96.8598	97.7330	97.1210	100.6009	90.4401	27.9841
G21	0.0000	0.0000	0.0000	0.0000	0.0000	0.0000	0.0000	0.0000	–0.0762
G31	0.0000	–10.5221	–12.2462	–13.2113	–13.2087	–13.0833	–13.5607	–10.4521	–7.5523
G12	0.0000	0.0000	0.0000	0.0000	0.0000	0.0000	0.0000	0.0000	–0.0762
G22	320.4100	338.3024	325.7303	326.1390	330.1852	325.1530	339.1122	330.8761	84.1439
G32	0.0000	0.0000	0.0000	0.0000	0.0000	0.0000	0.0000	0.0000	–0.4018
G13	0.0000	–10.5221	–12.2462	–13.2113	–13.2087	–13.0833	–13.5607	–10.4521	–7.5523
G23	0.0000	0.0000	0.0000	0.0000	0.0000	0.0000	0.0000	0.0000	–0.6967
G33	27.8784	28.5028	28.4622	27.8653	28.0582	27.9629	27.3948	28.4089	89.4916
G*11	0.0029	0.0114	0.0111	0.0110	0.0109	0.0110	0.0107	0.0115	0.0366
G*21	0.0000	0.0000	0.0000	0.0000	0.0000	0.0000	0.0000	0.0000	0.0001
G*31	0.0000	0.0042	0.0048	0.0052	0.0051	0.0051	0.0053	0.0042	0.0031
G*12	0.0000	0.0000	0.0000	0.0000	0.0000	0.0000	0.0000	0.0000	0.0001
G*22	0.0031	0.0030	0.0031	0.0031	0.0030	0.0031	0.0029	0.0030	0.0119
G*32	0.0000	0.0000	0.0000	0.0000	0.0000	0.0000	0.0000	0.0000	0.0001
G*13	0.0000	0.0042	0.0048	0.0052	0.0051	0.0051	0.0053	0.0042	0.0031
G*23	0.0000	0.0000	0.0000	0.0000	0.0000	0.0000	0.0000	0.0000	0.0001
G*33	0.0359	0.0366	0.0372	0.0384	0.0381	0.0382	0.0391	0.0368	0.0114

Table 3. The *d*-Spacing of Possible (hk0) of the Nine Minerals

Grunerite	**12 (hk0)**	(020)	(110)	(130)	(200)	(150)	(240)	(310)	(170)	(350)	(420)	(280)	(370)
	***d* (Å)**	9.197	8.341	5.129	4.679	3.424	3.280	3.076	2.530	2.379	2.267	2.064	2.010
Riebeckite	**12 (hk0)**	(020)	(110)	(130)	(200)	(150)	(240)	(310)	(260)	(170)	(350)	(420)	(280)
	***d* (Å)**	9.024	8.403	5.082	4.748	3.374	3.271	3.118	2.541	2.488	2.380	2.296	2.038
Tremolite	**12 (hk0)**	(020)	(110)	(130)	(200)	(150)	(240)	(310)	(170)	(350)	(420)	(280)	(370)
	***d* (Å)**	9.030	8.420	5.088	4.759	3.377	3.275	3.125	2.490	2.384	2.301	2.040	2.002
Actinolite	**12 (hk0)**	(020)	(110)	(130)	(200)	(220)	(150)	(240)	(310)	(170)	(350)	(420)	(280)
	***d* (Å)**	9.086	8.465	5.117	4.783	3.397	3.294	3.141	2.505	2.397	2.313	2.052	2.013
Anthophyllite	**20 (hk0)**	(200)	(020)	(210)	(220)	(230)	(410)	(240)	(430)	(250)	(610)		
	***d* (Å)**	9.250	8.950	8.218	6.432	5.014	4.478	4.028	3.655	3.339	3.039		
		(620)	(260)	(450)	(640)	(270)	(650)	(810)	(470)	(280)	(830)		
		2.915	2.839	2.831	2.539	2.465	2.336	2.293	2.238	2.175	2.156		
Winchite	**12 (hk0)**	(020)	(110)	(130)	(150)	(170)	(200)	(240)	(280)	(310)	(350)	(370)	(420)
	***d* (Å)**	9.016	8.452	5.090	3.375	2.487	4.784	3.281	2.039	3.141	2.389	2.004	2.312
Richterite	**13 (hk0)**	(020)	(110)	(130)	(200)	(150)	(240)	(310)	(170)	(350)	(420)	(280)	(370)	(190)
	***d* (Å)**	9.208	8.575	5.185	4.845	3.443	3.337	3.181	2.539	2.428	2.343	2.079	2.040	2.002
Cummingtonite	**11 (hk0)**	(020)	(110)	(130)	(200)	(150)	(240)	(310)	(170)	(350)	(420)	(280)		
	***d* (Å)**	9.905	8.284	5.080	4.653	3.388	3.252	3.058	2.503	2.360	2.254	2.043		
Talc	**13 (hk0)**	(020)	(110)	(130)	(200)	(150)	(240)	(310)	(170)	(350)	(420)	(280)	(370)	(510)
	***d* (Å)**	4.586	4.538	2.636	2.615	1.730	1.722	1.712	1.270	1.262	1.256	1.049	1.046	1.039

$$\cos\alpha^* = (\cos\beta\cos\gamma - \cos\alpha)/(\sin\beta\sin\gamma)$$
$$\cos\beta^* = (\cos\alpha\cos\gamma - \cos\beta)/(\sin\alpha\sin\gamma)$$
$$\cos\gamma^* = (\cos\alpha\cos\beta - \cos\gamma)/(\sin\alpha\sin\beta)$$

The *d*-spacing d of a crystallographic plane (h k l) is calculated by

$$1/d^2 = [h\ k\ l]\ [MT]^*\ [h\ k\ l]^t. \qquad \textbf{Equation 1}$$

The angle between two crystallographic planes ($h^1\ k^1\ l^1$) and ($h^2\ k^2\ l^2$) is calculated by

$$angle = \cos^{-1}\left([h_1\ k_1\ l_1]\ [MT]^*\ [h_2\ k_2\ l_2]^t/|h_1\ k_1\ l_1|\ |h_2\ k_2\ l_2|\right), \qquad \textbf{Equation 2}$$

where $[h_1\ k_1\ l_1]$, $[h_2\ k_2\ l_2]$ = the numerical values of Miller indices for the two planes, and $|h_1\ k_1\ l_1|$, $|h_2\ k_2\ l_2|$ = the magnitude of each plane perpendicular. The magnitude of the plane's perpendicular is calculated by $|h\ k\ l|^2 = [h\ k\ l]\ [MT]^*\ [h\ k\ l]^t$.

The angle between two crystallographic axes $[u_1\ v_1\ w_1]$ and $[u_2\ v_2\ w_2]$ is calculated by

$$angle = \cos^{-1}\left([u_1\ v_1\ w_1]\ [MT]\ [u_2\ v_2\ w_2]^t/|u_1\ v_1\ w_1|\ |u_2\ v_2\ w_2|\right), \qquad \textbf{Equation 3}$$

where $[u_1\ v_1\ w_1]$, $[u_2\ v_2\ w_2]$ = the numerical values of zone axes for the two axes, and $|u_1\ v_1\ w_1|$, $|u_2\ v_2\ w_2|$ = the magnitude of each axis. The magnitude of the axes is calculated by $|u\ v\ w|^2 = [u\ v\ w]\ [MT]\ [u\ v\ w]^t$.

All *d*-θ look-up tables in this paper were generated by Equations 1, 2, and 3.

The direct and reciprocal lattice cell parameters as well as the corresponding Metric Tensor [*MT*] and its inverse [*MT*]* of the nine minerals are summarized in Table 2.

2) The *d*-spacings of possible (hk0) of the nine minerals.

All asbestiform amphiboles elongate along *c*-axis, which is in most majority cases at a small angle to the specimen membrane's surface in TEM analysis. Therefore, there is always a (hk0) reciprocal diffraction spot

Table 4. An Example of *d*-*θ* Look-Up Table: The Partial Anthophyllite (2 0 0)

Anthophyllite (2 0 0) 288 Zone Axes

a - *18.50*Å, *b* - *17.90*Å, *c* - 5.28Å, α - 90°, β - 90°, γ - 90°

Space Group Pnma *h=2n* for *(hk0)*; *(k+l)=2n* for *(0kl)*

[U V W]	(h k 0)	(h k l)	*d*(hk0)	*d*(hkl)	*d* Ratio	θ °	ZA^C°
[0 2 1]	(2 0 0)	(1 1 2)	9.250	2.586	3.58	82.0	81.6
[0 –1 2]	(2 0 0)	(6 2 1)	9.250	2.552	3.62	34.1	59.5
[0 –2 –1]	(2 0 0)	(2 –1 2)	9.250	2.513	3.68	74.2	81.6
[0 –1 1]	(2 0 0)	(1 2 2)	9.250	2.509	3.69	82.2	73.6
[0 –1 3]	(2 0 0)	(6 3 1)	9.250	2.431	3.80	37.9	48.5
[0 1 0]	(2 0 0)	(3 0 2)	9.250	2.427	3.81	66.8	90.0
[0 –2 1]	(2 0 0)	(3 1 2)	9.250	2.405	3.85	67.0	81.6
[0 –2 3]	(2 0 0)	(1 3 2)	9.250	2.394	3.86	82.6	66.1
[0 1 0]	(2 0 0)	(7 0 1)	9.250	2.363	3.91	26.6	90.0
[0 –1 1]	(2 0 0)	(7 1 1)	9.250	2.343	3.95	27.6	73.6
[0 –1 1]	(2 0 0)	(3 2 2)	9.250	2.342	3.95	67.7	73.6
[0 –2 3]	(2 0 0)	(2 3 2)	9.250	2.336	3.96	75.4	66.1
[0 –2 1]	(2 0 0)	(4 1 2)	9.250	2.274	4.07	60.5	81.6
[0 –2 –1]	(2 0 0)	(–4 –1 2)	9.250	2.274	4.07	60.5	81.6
[0 –1 2]	(2 0 0)	(0 4 2)	9.250	2.274	4.07	90.0	59.5
[0 –1 –2]	(2 0 0)	(1 –4 2)	9.250	2.257	4.10	83.0	59.5
[0 –2 3]	(2 0 0)	(3 3 2)	9.250	2.248	4.11	68.6	66.1
[0 –2 3]	(2 0 0)	(4 3 2)	9.250	2.140	4.32	62.4	66.1
[0 –2 –3]	(2 0 0)	(–4 –3 2)	9.250	2.140	4.32	62.4	66.1
[0 –2 1]	(2 0 0)	(5 1 2)	9.250	2.134	4.34	54.8	81.6
[0 –2 –1]	(2 0 0)	(–5 –1 2)	9.250	2.134	4.34	54.8	81.6
[0 –1 2]	(2 0 0)	(3 4 2)	9.250	2.133	4.34	69.8	59.5
[0 1 0]	(2 0 0)	(8 0 1)	9.250	2.118	4.37	23.7	90.0
[0 –2 5]	(2 0 0)	(1 5 2)	9.250	2.111	4.38	83.4	53.6
[0 –1 1]	(2 0 0)	(8 1 1)	9.250	2.104	4.40	24.5	73.6
[0 –1 1]	(2 0 0)	(5 2 2)	9.250	2.090	4.43	55.6	73.6
[0 –2 5]	(2 0 0)	(2 5 2)	9.250	2.071	4.47	77.1	53.6

row that represents a group of direct lattice planes, which are parallel to *c*-axis regardless of the zone-axis orientation. The possible (hk0)s are summarized in Table 3, which were generated by Equation 1 with cut-off values set at 2 Å for amphibole and 1 Å for talc. All *d*-*θ* look-up tables are organized according to (hk0).

3) An example of *d*-*θ* look-up table (Table 4).

4) The structure of *d*-*θ* look-up tables (Table 5).

HOW TO USE THE *d*-*θ* LOOK-UP TABLE

The stepwise procedure of using the *d*-*θ* look-up table for indexing and interpreting a zone-axis SAED pattern can be illustrated by the following example (15) in Figure 1.

1) *Establish the mineral's* ***identity***: The mineral was identified to be riebeckite (crocidolite) by TEM imaging and EDS analysis.

2) *Measure two* ***d-spacings***: Measure the *d*-spacings of two intersecting diffraction spot rows, i.e., images of direct lattice planes:

- preferably, but not necessarily, two shortest *d*-spacings, e.g., the two lines in Figure 1;
- at this point we don't know which is the (hk0) row except in the case that the fiber orientation relative to the pattern is known, and therefore the diffraction spot row parallel to the fiber elongation, i.e., *c*-axis, is the (hk0) row. Nor can we assume that the diffraction spot row with smaller geometric spacing or greater *d*-spacing must be the (hk0) row because that is not al-

Table 5. The Structure of *d*-θ Look-Up Tables

Column	Description	Remarks
[U V W]	The direct crystal axis parallel to the electron beam at the orientation when the SAED pattern is recorded. It is the intersection line between the (hk0) and (hkl) direct lattice planes listed in the following two columns, respectively.	Mathematically, it is the cross product of the two matrices represented by the Miller Indices of direct lattice planes (hk0) and (hkl) listed in the following two columns, respectively. It is also the path of incident electron beam.
(hk0)	The Miller index of the direct lattice plane (hk0).	—
(hkl)	The Miller index of the direct lattice plane (hkl).	—
d(hk0)	The *d*-spacing along the (hkl) layer line, which equals the inverse of the perpendicular geometric distance between two adjacent direct lattice planes divided by the diffraction camera constant.	Measured by a fine ruler with 0.5 mm divisions from SAED patterns and calculated by the equation: *d* = (diffraction camera constant / geometrical distance between adjacent diffraction spots).
d(hkl)	The *d*-spacing along the (hkl) layer line, which equals the inverse of the perpendicular geometric distance between two adjacent direct lattice planes divided by the diffraction camera constant.	Measured by a fine ruler with 0.5 mm divisions from SAED patterns and calculated by the equation: *d* = (diffraction camera constant / geometrical distance between adjacent diffraction spots).
d ratio	The ratio of *d*(hk0) to *d*(hkl)	*d*(hk0) / *d*(hkl)
θ (°)	The acute interplanal angle between the intersecting direct lattice planes (hk0) and (hkl).	Measured by a fine goniometer with 0.5° divisions from the pattern.
ZA^c (°)	The angle between the electron beam and the direct crystallographic *c*-axis.	The amphibole fiber's elongation axis, i.e. *c*-axis, is usually at low angles (0° to ~30°) to the filter surface. Even if the filter is tilted to align to a zone axis, the angle between the tilted fiber and the electron beam, which is the direction of zone axis, is unlikely less than 45°. Therefore, only ZA^c ≥ 45° is listed. For talc, there is no restriction on ZA^c values.

ways the case. For example, as shown in Figure 2, the [0 1 0] zone axis pattern formed by (2 0 0) and (0 0 1) has a (hk0) with smaller *d*-spacing than that of (hkl);

• with a 0.5 mm-division fine ruler and read the distance between two adjacent spots to the first decimal place in millimeters, spanning to as many as possible spots across the pattern to improve accuracy;

• the 6.60 mm and 3.81 mm distances were converted through the diffraction camera constant 31.94 mm·Å into *d*-spacings of 31.94/6.60 = 4.89 Å and 31.94/3.81 = 8.38 Å, respectively;

3) *Measure the* ***interplanar angle***: Measure the angle between the two measured intersecting diffraction spot rows, i.e., two intersecting direct lattice planes: $\theta = 82.5°$.

4) *Search Table 2 for* ***possible (hk0)s***:

• look up in riebeckite row;

• find the *d*-spacings close to the observed (hk0) values 4.89 Å and 8.38 Å, i.e., (2 0 0) – 4.75 Å and (1 1 0) 8.40 Å, respectively;

• calculate the *R* values for (2 0 0) *R* = 4.89/8.38 = 0.58 and for (1 1 0) *R* = 8.38/4.89 = 1.73. Remember that the *d*-spacing is inversely proportional to the geometrical distance between diffraction spots, i.e., the reciprocal lattice points.

5) *Search the* ***first (hk0) table***: Compare the observed *d*(hk0)-*d*(hkl)-*R*-θ combination (4.89-8.38-0.58-82.5) against the first possibility riebeckite (2 0 0) *d*-θ look-up table (Figure 2). Obviously, no match could be found. For (2 0 0), the greatest *d*(hkl) is only 5.186, far less than the observed 8.38. There is no match either for *R*-θ in the whole (2 0 0) table.

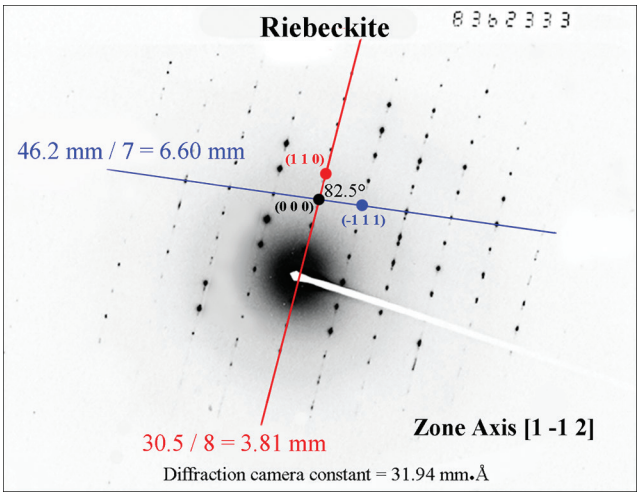

Figure 1. The [1 –1 2] zone-axis SAED pattern of the riebeckite from the collection of NIST Standard Reference Material, 1866 (15).

6) *Search the* ***second (hk0) table***: Compare the observed *d*(hk0)-*d*(hkl)-*R*-*θ* combination (8.38-4.89-1.73-82.5) against the second possibility riebeckite (1 1 0) look-up table (Figure 3). An exclusive match for *d*-spacing is found to be (hk0) = (1 1 0) –8.40 Å and (hkl) = (–1 1 1) – 4.89 Å, whereas both *R* and *θ* are also very close. Therefore, the zone axis of this pattern is [1 –1 2].

7) *Confirm the mineral's* ***identity***: The identity of riebeckite is now confirmed by the conformance of the analyzed zone-axis SAED pattern to riebeckite's crystal structure.

WHAT IF THE DIFFRACTION CAMERA CONSTANT IS NOT AVAILABLE?

Sometimes, the diffraction camera constant associated with a zone-axis SAED pattern may be missing or the orientation of the fiber may also be missing. In this case, it is still possible to index and solve the pattern by only *θ* and *R* data (15). Figure 4 is a well-oriented zone-axis SAED pattern of grunerite (amosite) as identified by its TEM image and EDS spectrum, published by Japan Electron Optics Laboratory (16) without the information of the associated diffraction camera constant and the identification of its zone axis.

The pattern was enlarged on a computer screen, and two diffraction spot rows were selected and measured as red = 5.8 mm and blue = 10.2 mm (Figure 5). The angle *θ* between them was measured to be 90.0°. Not knowing which one is (hk0), the entire 12 *d*-*θ* look-up tables of grunerite in Table 2 were searched by two possibilities: *R* = 5.8/10.2 = 0.57 and *R* = 10.2/5.8 = 1.76. While the first *R*-*θ* combination (*0.57–90.0*) yielded no match at all, the second combination (*1.76–90.0*) produced a unique match: *(hk0) = (0 2 0) – 9.197 Å*, *(hkl) = (0 0 1) – 5.224 Å*, *R = 1.76*, and *θ = 90.0°* in the grunerite (0 2 0) *d*-*θ* look-up table (Figure 6), and the corresponding zone axis is therefore indexed as [1 0 0], which indicates that the pattern conforms to the grunerite crystal structure.

R-*θ* can be used to solve a zone-axis SAED pattern without the associated diffraction camera constant because *R* and *θ* are independent of the diffraction camera constant and much less susceptible than the absolute *d*(hk0) and *d*(hkl) values to the compositional differences between the tested specimen and the reference material used to generate the *d*-*θ* look-up tables (15). Therefore, even in the normal case that *d*-spacing data are available, a greater weight should be placed on *R* and *θ* values than the absolute *d*-spacing values in the search of *d*-*θ* look-up tables.

THE CALCULATION OF ZONE AXIS AND THE APPEARANCE OF NONCONFORMANCE TO WEISS ZONE LAW

After a positive match is found in the *d*-*θ* look-up tables, the corresponding zone axis is listed on the same line, which can also be calculated by hand as follows (Figure 7):

The mathematical relationship between the Miller index of lattice plane (hk0) or (hkl) and that of the corresponding zone axis, which is the intersection of (hk0) and (hkl), is governed by Weiss zone law (17):

$$u \times h + v \times k + w \times l = 0.$$

For example, the riebeckite in Figure 3:

$$(\mathbf{1} \times 1 + \mathbf{-1} \times 1 + \mathbf{2} \times 0) = 0;\ (\mathbf{1} \times -1 + \mathbf{-1} \times 1 + \mathbf{2} \times 1) = 0.$$

However, sometimes it is possible that a zone axis's Miller index will not conform to the Weiss zone law. For example, a tremolite's pattern is indexed as (hk0) = (2 0 0) and (hkl) = (1 1 1), whose corresponding zone axis is then calculated to be u = *(0 × 1 – 0 × 1) = 0*; v = *(0 × 1 – 2 × 1) = –2*; w = *(2 × 1 – 0 × 1) = 2*. Therefore, [u v w] should be [0 –2 2] or [0 –1 1]. One may find that the zone axis is actually written as [0 1 1], which does not follow the Weiss zone law because $(\mathbf{0} \times 1 + \mathbf{1} \times 1 + \mathbf{1} \times 1) \neq 0$. This is not a nonconformance of Weiss zone law because tremolite is monoclinic and has a symmetric plane (0 1 0). Because it is impossible

Riebeckite (200) 187 Zone Axes

a 9.769Å *b* 18.048Å *c* 5.335Å *α* 90° *β* 103.59° *γ* 90°

Space Group C2/m permits only *(h+k)=2n*

[U	V	W]	(h	k	0)	(h	k	l)	*d* (hk0)	*d* (hkl)	*d* Ratio	*θ*°	ZA^C°
[0	1	0]	(2	0	0)	(0	0	1)	4.748	5.186	0.92	76.4	90.0
[0	1	1]	(2	0	0)	(1	1	-1)	4.748	4.891	0.97	72.9	73.5
[0	-1	-2]	(2	0	0)	(0	-2	1)	4.748	4.496	1.06	78.2	59.4
[0	-1	1]	(2	0	0)	(1	1	1)	4.748	4.052	1.17	52.4	73.5

Figure 2. The partial (2 0 0) *d-θ* look up table of riebeckite.

Parameter	$d_{(hk0)}$	$d_{(hkl)}$	$R\ (d_{(hk0)}/d_{(hkl)})$	θ
Observed	***3.81 mm*** ***8.38 Å***	***6.60 mm*** ***4.84 Å***	***1.73***	***82.5 °***
Reference	8.40 Å	4.89 Å	1.72	82.3°
Deviation	0.02	0.05	0.01	0.2
	0.2%	1.0%	0.6%	0.2%
Conclusion	**(1 1 0)**	**(-1 1 1)**	Zone Axis = **[1 -1 2]**	

Riebeckite (110) 362 Zone Axes

a 9.769Å *b* 18.048Å *c* 5.335Å *α* 90° *β* 103.59° *γ* 90°

Space Group C2/m permits only *(h+k)=2n*

[U	V	W]	(h	k	0)	(h	k	l)	*d* (hk0)	*d* (hkl)	*d* Ratio	*θ*°	ZA^C°
[1	-1	0]	(1	1	0)	(0	0	1)	8.403	5.186	1.62	78.0	83.6
[1	-1	2]	(1	1	0)	(-1	1	1)	8.403	4.891	1.72	82.3	67.7
[1	-1	0]	(1	1	0)	(1	1	-1)	8.403	4.891	1.72	67.3	83.6
[1	-1	2]	(1	1	0)	(0	2	1)	8.403	4.496	1.87	65.7	67.7

Figure 3. The partial (1 1 0) *d-θ* look-up table of riebeckite.

to distinguish the crystallographic axis *b*s positive end from its negative end, [0 –1 1] is equal to [0 1 1].

Based on the crystal's symmetry, the zone-axis equivalency rules are summarized in Table 6. For monoclinic amphibole asbestos, i.e., grunerite, riebeckite, tremolite, and actinolite, (0 1 0) is a symmetric plane. One can change the sign of v, whose direction is perpendicular to (0 1 0), in any u/v/w combination without changing the zone axis's actual orientation in the crystal. For orthorhombic amphibole asbestos, i.e., anthophyllite, there is a symmetric center. One can change every negative sign in any u/v/w combination without changing the zone axis's actual orientation in the crystal. Therefore, if a zone axis appears to not conform to Weiss zone law, check whether it is a true error or an equivalent zone axis due to symmetry.

EVALUATING THE POSITIVE MATCH BETWEEN THE OBSERVED AND REFERENCE *d-θ* VALUES

Although the above-mentioned, two randomly selected examples show a positive match more or less than 1% between the observed and reference *d-θ-R* values, it does not imply that the acceptable tolerance must be that strict. Then, what will be a reasonable and objective tolerance for evaluating the positive match between the observed and reference *d-θ* values?

Let's take a look at an extreme case: the *d-θ* variations as a result of isomorphic iron substitution from tremolite to actinolite (Table 7). When half of Mg2+ (radius 0.072 nm) in tremolite is replaced by the larger Fe2+ (radius 0.077 nm) to form actinolite, the crystal's cell dimension is accordingly expanded, resulting in the increase of the length of crystallographic axes *a*, *b*, and *c* plus the change of the angle *β* between *a* and *c*. We know that the *d-θ* values are entirely determined by the cell dimension or six cell parameters, the expansion of the cell dimension will propagate to the variations of all *d*-spacings and *θ*. Even though it is a big jump in terms of compositional change from one end-member tremolite to the other end-member actinolite in this isomorphic series, none of the net changes of *d-θ* values is more than 1.09%. In the real world, the chemical composition change among the same species from different geological environments will likely be less than that of the tremolite-actinolite case, i.e., maximum change from one end member to the other in an isomorphic series.

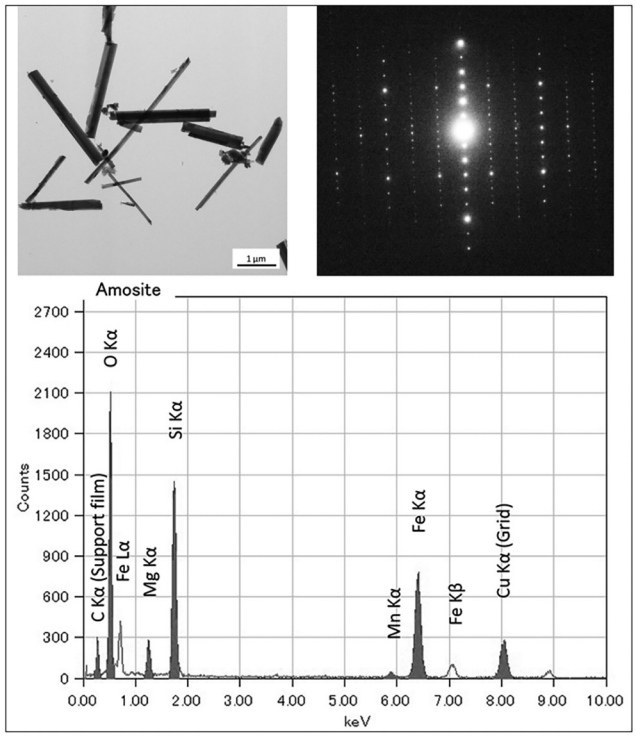

Figure 4. The JEOL grunerite (16).

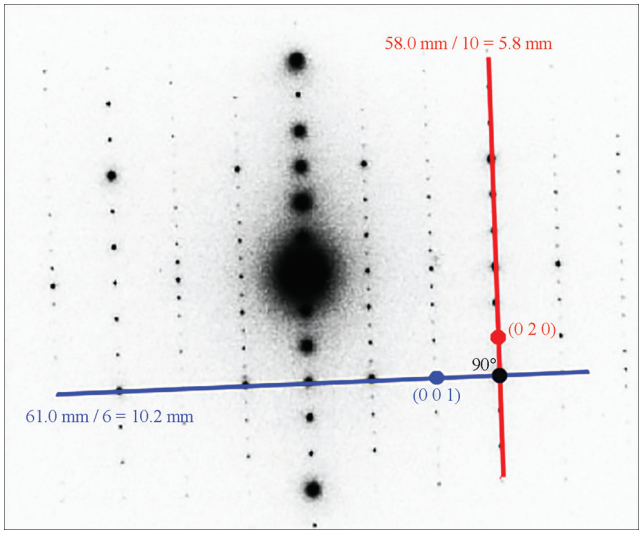

Figure 5. The indexed grunerite SAED pattern in Figure 4.

However, we must distinguish the two types of parameters: one that is independent of the diffraction camera constant, i.e., $R = d_{(hk0)}/d_{(hkl)}$ and θ, and the other that is dependent on the accuracy of diffraction camera constant, i.e., $d_{(hk0)}$ and $d_{(hkl)}$.

Based on Table 7 and many real-world examples, it can be concluded that a 2% tolerance will be a scientifically objective criterium for evaluating the positive match between the observed and reference d-θ values for parameters independent of diffraction camera constant, i.e., $R = d_{(hk0)}/d_{(hkl)}$ and θ, whereas up to 5% tolerance maybe acceptable for absolute d-spacing values that are dependent on the measurement errors of diffraction camera constant.

COMPARISON WITH A HISTORICAL VERSION OF d-θ TABLES

The first set of five regulated amphibole asbestos tables was created yet never formally published by Dr. Robert J. Stevenson, McCrone Associates, in the 1980s. Because its limited number of zone axes was insufficient to cover patterns encountered by asbestos analysts in their daily work, this author created a new set of d-θ tables for the five regulated amphibole asbestos minerals with much wider ranges of zone axis in 1993 and later two Libby (Montana) amphiboles in 2001, which were also never formally published but have been widely used by the asbestos analysis community ever since. During the author's career of assessing hundreds of National Voluntary Laboratory Accreditation Program's (NVLAP) TEM laboratories over the past three decades in the U.S., Canada, and Asia, many unsolvable zone-axis SAED patterns were encountered. Obviously, the 1993/2001 tables are not comprehensive enough to solve some SAED patterns seen by asbestos analysts in their routine work because not all possible (hk0) and (hkl) were covered in those tables.

As shown in Table 8, this new set of tables is much more comprehensive (more than 800 pages and 36,000 zone axes) and, in theory, covers all possible (hk0) and (hkl) planes, containing thousands of zone axes for each of the nine minerals. For the first time, this publication marks the creation of talc and cummingtonite tables, which were previously unavailable.

SUMMARY

1) The practical and effective way to solve amphibole zone-axis SAED patterns in TEM asbestos analysis is to first establish the identity of mineral fiber by morphological and chemical information and then compare the measured d-θ data against the corresponding pre-calculated d-θ look-up tables organized by d(hk0) values.

2) When comparing, give priority to θ and R, which are independent of the measurement errors of

Parameter	$d_{(hk0)}$	$d_{(hkl)}$	$R\ (d_{(hk0)}/d_{(hkl)})$	θ
Observed	***5.8 mm***	***10.2 mm***	***1.75(9)***	***90.0 °***
Reference	9.197 Å	5.224 Å	1.76(0)	90.0°
Deviation			0.00(1)	0.0
			0.1%	0.0%
Conclusion	**(0 2 0)**	**(0 0 1)**	Zone Axis = **[1 0 0]**	

Grunerite (020) 175 Zone Axes

a 9.564Å ***b*** 18.393Å ***c*** 5.339Å ***α*** 90° ***β*** 101.9° ***γ*** 90°

Space Group C 2/m permits only *(h+k)=2n*

[U V W]	(h k 0)	(h k l)	*d* (hk0)	*d* (hkl)	*d* Ratio	*θ*°	ZA^C°
[1 0 0]	(0 2 0)	(0 0 1)	9.197	5.224	1.76	90.0	78.1
[1 0 1]	(0 2 0)	(1 1 -1)	9.197	4.846	1.90	74.7	70.2
[1 0 0]	(0 2 0)	(0 -2 -1)	9.197	4.542	2.02	60.4	78.1
[1 0 -1]	(0 2 0)	(1 1 1)	9.197	4.102	2.24	77.1	52.0

Figure 6. The partial grunerite (0 2 0) *d*-θ look-up table.

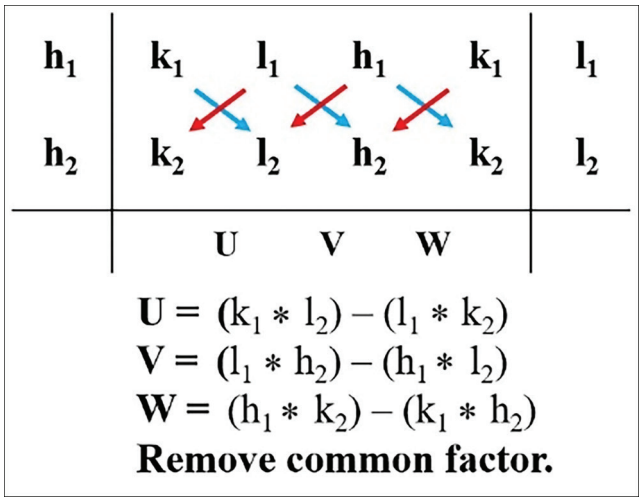

Figure 7. Using the Miller indices of (hk0) and (hkl) to calculate the Miller index [U V W] of the corresponding zone axis.

diffraction camera constant and less susceptible to the compositional difference between the tested specimen and the reference material.

3) It is possible to solve a zone-axis SAED pattern without the knowledge of the associated diffraction camera constant by using *R*-θ.

4) When the Miller index of a zone axis doesn't conform to Weiss zone law, it may still be correct because of the equivalency rules governed by the crystal's symmetry.

5) Pre-calculated *d*-θ look-up tables can be readily generated by algorithms based on the Metric Tensor [*MT*] and its inverse [*MT*]*.

6) The objective and practical tolerances for evaluating the positive match between the observed and reference *d*-θ values are 2% for parameters independent of diffraction camera constant, i.e., $d_{(hk0)}/d_{(hkl)}$ and θ, and 5% for parameters dependent on diffraction camera constant, i.e., $d_{(hk0)}$ and $d_{(hkl)}$.

7) This publication presents not only the hitherto most comprehensive set of *d*-θ tables for amphiboles (29,000-plus zone axes) but also the first set of talc (3,000-plus zone axes) and cummingtonite (3,000-plus zone axes) tables ever created.

8) Not only this methodology is applicable to the traditional airborne asbestos analysis, it is equally applicable to all asbestos analysis by TEM, such as asbestos in water, dust, bulk, human tissue, etc.

ACKNOWLEDGMENTS

I would like to dedicate this paper to the memory of Dr. Huayi Zhang, Renaissance Capital. His inspiration is the reason of my research work involving extensive programming, especially this one. Constructive contributions from Dr. Mickey E. Gunter, University Distinguished Professor Emeritus at University of Idaho, are highly appreciated. Valuable comments by Dr. James R. Millette, Executive Director at Millette Technical Consulting, have substantially improved this paper.

REFERENCES CITED

1. Dyar, M.D. and Gunter, M.E. *Mineralogy and Optical Mineralogy*, 2nd Edition, Mineralogical Society of America: Chantilly, VA, 708 pp, 2019.

2. Hahn, T. *International Tables for Crystallography: Volume A — Space Group Symmetry*, 4th Edition, International Union of Crystallography, Kluwer Academic Publishers: Dordrecht, the Netherlands, 1996.

3. U.S. EPA. Interim Transmission Electron Microscopy Analytical Methods — Mandatory and Non-

Table 6. The Equivalency of Zone Axis for Monoclinic and Orthorhombic Systems

Monoclinic (010) Symmetrical Plane	Orthorhombic Symmetrical Center
[u v w] = [u –v w] = [–u v –w] = [–u v –w] = [–u –v –w]	[u v w] = [u –v w] = [u –v –w] = [u v –w] = [–u v w] = [–u –v w] = [–u –v –w]
[u –v –w] = [u v –w]	
[–u v w] = [–u –v w]	

Table 7. The *d*-θ Variations Due to Cell Parameter Changes Caused by Isomorphic Iron Substitution from Tremolite to Actinolite

Mineral	Tremolite	Actinolite	Net Change	% of Change
Composition	$Ca_2Mg_5(Si_8O_{22})(OH)_2$	$Ca_2(Mg_{2.5}Fe_{2.5})Si_8O_{22}OH_2$	$Fe_{2.5}$	50% of Mg
System	Monoclinic	Monoclinic	None	N/A
a (Å)	9.840	9.860	–0.020	–0.20
b (Å)	18.020	18.110	–0.090	–0.50
c (Å)	5.270	5.340	–0.070	–1.31
α (°)	90.000	90.000	0.000	0.00
β (°)	104.900	105.000	–0.100	–0.10
γ (°)	90.000	90.000	0.000	0.00
$d_{(020)}$ (Å)	9.010	9.055	–0.045	–0.50
$d_{(021)}$ (Å)	4.433	4.482	–0.049	–1.09
$d_{(020)} / d_{(021)}$	2.03	2.02	0.01	0.50
θ (°)	60.5	60.3	0.20	0.33

Table 8. The Numbers of Zone Axis in the Historical and Current Versions

Mineral Name	No. of (hk0)		No. of Zone Axis	
	1993	2021	1993	2021
Grunerite	8	12	983	3,515
Riebekite	7	12	830	3,560
Tremolite	7	11	803	3,378
Actinolite	7	12	813	3,451
Anthophyllite	15	20	1,386	7,785
Winchite	9*	13	802*	3,544
Richterite	8*	13	1,940*	3,898
Cummingtonite	N/A	11	N/A	3,076
Talc	N/A	13	N/A	3,882

*2001

mandatory — and Mandatory Section to Determine Completion of Response Actions. 40 CFR, Appendix A to Subpart E of Part 763, 1987.

4. Palmer, D.C. *SingleCrystal User's Guide*, Version 4, CrystalMaker Software Ltd., 190 pp, 2020.

5. Warren, B. and Modell, D. "The Structure of Anthophyllite H_2 Mg_7 (Si $O_3)_8$," *Zeitschrift fur Kristallographie*, 75, pp 161–179, 1930.

6. Finger L.W. "*The Crystal Structure and Cation Distribution of a Grunerite. Locality: Wabush Iron Formation, Labrador, Canada*," Mineralogical Society of America Special Paper 2, pp 95–100, 1969.

7. Hawthorne, F.C. "The Crystal Chemistry of the Amphiboles; VIII, The Crystal Structure and Site Chemistry of Fluor-riebeckite," *The Canadian Mineralogist*, 16, pp 187–194, 1978.

8. Ballirano, P.; Andreozzi, G.B.; and Belardi, G. "Crystal Chemical and Structural Characterization of Fibrous Tremolite from Susa Valley, Italy, with Comments on Potential Harmful Effects on Human Health," *American Mineralogist*, pp 1349–1355, 2008.

9. Evans, B.W. and Yang, H. "Fe-Mg Order-Disorder in Tremolite-Actinolite-Ferro-actinolite at Ambient and High Temperature," *American Mineralogist*, 83, pp 458–475, 1998.

10. Wylie, A.G. and Verkouteren, J.R. "Amphibole Asbestos from Libby, Montana: Aspects of Nomenclature," *American Mineralogist*, 85, pp 1540–1542, 2000.

11. Ventura, G.D.; Robert, J-L; Raudsepp, M.; and Hawthorne, F.C. "Site Occupancies in Monoclinic Amphiboles: Rietveld Structure Refinement of Synthetic Nickel Magnesium Cobalt Potassium Richterite," *American Mineralogist*, 78, pp 633–640, 1993.

12. Fisher, K.F. "A Further Refinement of the Crystal Structure of Cummingtonite $(Mg,Fe)_7(Si_4O11)_2(OH)_2$, *American Mineralogist*, 51, pp 814–818, 1966.

13. Perdikatsis, B. and Burzlaff, H. "Strukturverfeinerung am Talk $Mg_3[(OH)_2Si_4O_{10}]$," *Zeitschrift fur Kristallographie*, 156, pp 177–186, 1981.

14. Boisen, M.B. and Gibbs, G.V. "Mathematical Crystallography — An Introduction to the Mathematical Foundations of Crystallography," *Mineralogical Society of America*, Reviews in Mineralogy, Vol. 15; Paul H. Ribbe, Ed., xii + 406 pp, 1985.

15. NIST SRM. "Certificate, Standard Reference Material 1866," National Institute of Standards and Technology, 1988.

16. JEOL. "Analysis of Asbestos — Distinguish Fine Fibers One by One," Application Note EM057, 2018.

17. Bloss, F.D. *Crystallography and Crystal Chemistry*, Holt, Rinehart and Winston: New York and London, xiv + 543 pp, 1971. ■